Layered, Nanonetwork Composite Cathodes for Flexible, High-Efficiency, Organic Light Emitting Devices

*Junwei Xu, Gregory M. Smith, Chaochao Dun, Yue Cui, Jiwen Liu, Huihui Huang, Wenxiao Huang, and David L. Carroll**

In this work, the application of an aluminum (Al)/multiwall carbon nanotube (MWCNT)/Al, multilayered electrode to flexible, high-efficiency, alternating current driven organic electroluminescent devices (AC-OEL), is reported. The electrode is fabricated by sandwiching a spray-cast nanonetwork film of MWCNTs between two evaporated layers of Al. The resulting composite film facilitates a uniform charge distribution across a robust crack-free electrode under various bending angles. It is demonstrated that these composite electrodes stabilize the power efficiency of flexible devices for bending angles up to 120°, with AC-OEL device power efficiencies of ≈22 lm W^{-1} at luminances of ≈4000 cd m^{-2} (using no output coupling). Microscopic examination of the Al/MWCNTs/Al electrode after bending of up to 1300 cycles suggests that the nanotubes significantly enhance the mechanical properties of the thin Al layers while providing a moderate modification to the work function of the metal. While the realization of robust, high-brightness, and high-efficiency AC-OEL devices is potentially important in their future lighting applications, it is anticipated that this to also have significant impact in standard organic light emitting diodes lighting applications.

1. Introduction

Alternating current (AC) driven organic electroluminance (OEL) devices have received tremendous interest lately by the organic lighting community.[1–6] The devices which use an AC field to create polarization currents in an electroluminescent organic layer and thus generate light emission [7–10] have shown promise as high-quality panel lighting due to their property of simultaneously increasing brightness and power efficiency.[11–13] Furthermore, they may present potential advantages in driver circuit simplicity when interfacing to standard AC power sources. However, as with all ultrathin or organic lighting approaches, a widely sought property of the AC-OEL is flexibility.

The concept of low-cost, flexible, high-efficiency light sources based on organic solid-state lighting devices is already well established.[14–19] Indeed, both standard organic light emitting diodes (OLEDs) as well as AC-OELs have demonstrated brightness and efficiency numbers of commercial interest. However, the slow transition from state-of-the-art laboratory research to a modern manufacturing environment should somehow indicate the magnitude of the challenges faced by the technologies to meet with robust utilization in the consumer world.[20] Two key problems that developers are facing are addressed in this work.

The first is how to achieve extremely high-power efficiencies in lighting devices when internal quantum efficiencies are already reaching levels approaching 100% (both the spin-symmetric and antisymmetric molecular excitations are fully used for photon emission.[21–25] In any organic EL device, there are many energy loss mechanisms from carrier transport to multiple nonradiative processes that convert singlet and triplet excitations into the ground state.[21–24] Among these mechanisms, an important problem in OLEDs is direct injection of hot carriers, which form bound electron-hole pairs or excitons after tunneling through energy barriers at multiple interfaces.[26–29] These hot carriers exceed the energy gap of the emitting material, so the excess energy is wasted thermally, giving rise to a lower power efficiency. The reduction of the carrier injection barrier by decreasing the difference between adjacent energy levels (highest occupied molecular orbital (HOMO) or lowest unoccupied molecular orbital (LUMO)) is now a common method to optimize the efficiency of OLEDs.[30–34] However, as in the case with most technology demonstrators, what works best in the lab is difficult to implement in commercial settings, so placing Li or Ca at the metal interface is undesirable.

In the case of capacitively coupled AC-OEL devices, as described here, the large induced polarization currents effectively control the rate and energy of carrier "injection." While power efficiencies as high as 29.3 lm W^{-1} at 20 500 cd m^{-2} have been reported in green phosphorescent AC-OEL devices, it has

J. Xu, G. M. Smith, C. Dun, Y. Cui, Dr. J. Liu, Dr. H. Huang, W. Huang, Prof. D. L. Carroll
Center for Nanotechnology and Molecular Materials
Department of Physics
Wake Forest University
Winston-Salem, NC 27109, USA
E-mail: carroldl@wfu.edu

Y. Cui
Key Laboratory of Luminescence and Optical Information
(Ministry of Education)
Institute of Optoelectronics Technology
Beijing Jiaotong University
Beijing 100044, P. R. China

DOI: 10.1002/adfm.201501068

been anticipated that higher values are possible using asymmetric contact designs that allow for better charge compensation in the devices.[2,7,13] But it must be recognized that facile charge compensation in such asymmetric devices also requires engineering of the work function at the metal contact. And, again, we wish to avoid the use of typical laboratory solutions to this problem such as Li or Ca.

The second problem we would like to address is what the ideal flexible, reflective electrode for organic devices might be. A great deal of research has been devoted to the development of highly flexible electrodes with high transparency including metal nanowire grids,[35–40] graphene sheets,[41–45] and carbon nanotube (CNT) networks.[46–49] However, development of flexible cathode materials (the back reflector) with excellent optical, electrical, and mechanical properties is rarely reported. Generally, flexible optoelectronics, such as OLEDs and organic solar cells, utilize surprisingly thin metal layers as the flexible back cathode. Metals that have been most widely studied for this use include Al,[14,15] calcium (Ca)/Al,[50] nickel–chromium (Ni–Cr),[51] and sliver (Ag).[52] Interestingly, the balance between flexibility and conductivity is difficult to achieve. Metal electrodes can have residual stress due to work hardening and become rigid or brittle, leading unavoidably to cracking after repeated bending or stretching. Voids, gaps, and uneven thin film morphologies that result can then lead to nonuniform current distributions in the electrodes: essential for performance in both AC and DC EL devices. In the laboratory setting, one would choose the metal with most desirable mechanical properties then modify its work function using the methods described above. However, again, in a commercial sense this may not be possible.

To address the two challenges above, we examine the application of novel composite electrode structures, composed of metal/nanowires (nanotubes)/metal. We demonstrate that as a reliable alternative structure for the cathode, this triple-layer composite electrode gives an excellent balance between mechanical stability, electrical conductivity, and optical functionality even after thousands of bending cycles. We further demonstrate these Al (50 nm)/multiwall carbon nanotubes (MWCNTs)/Al (100 nm) cathodes on a flexible AC-OEL device structure which achieves and maintains a power efficiency of ≈22.2 lm W^{-1} at 4050 cd m^{-2} after full bending cycles of 120° for 10 min. However, we emphasize the generality of this approach and their potential use in OLEDs as well.

2. Results and Discussion

Figure 1a shows a diagram of the capacitive flexible AC-driven OEL device with a triple-layer composite cathode. The fabrication of the device starts with a clean polyethylene terephthalate (PET) substrate precoated with 100 nm of indium tin oxide (ITO). Commercial poly(3,4-ethylenedioxythiophene)-poly(styrenesulfonate) (PEDOT:PSS) doped with 36 wt% zinc oxide (ZnO) nanoparticles (NPs) (35 nm average diameter) is spun cast on ITO as not only a hole generation layer, but also as an inorganic semiconductor gate, which is required for a field-induced EL device. A more complete discussion and analysis of the function of insulating or semiconducting gate layers in

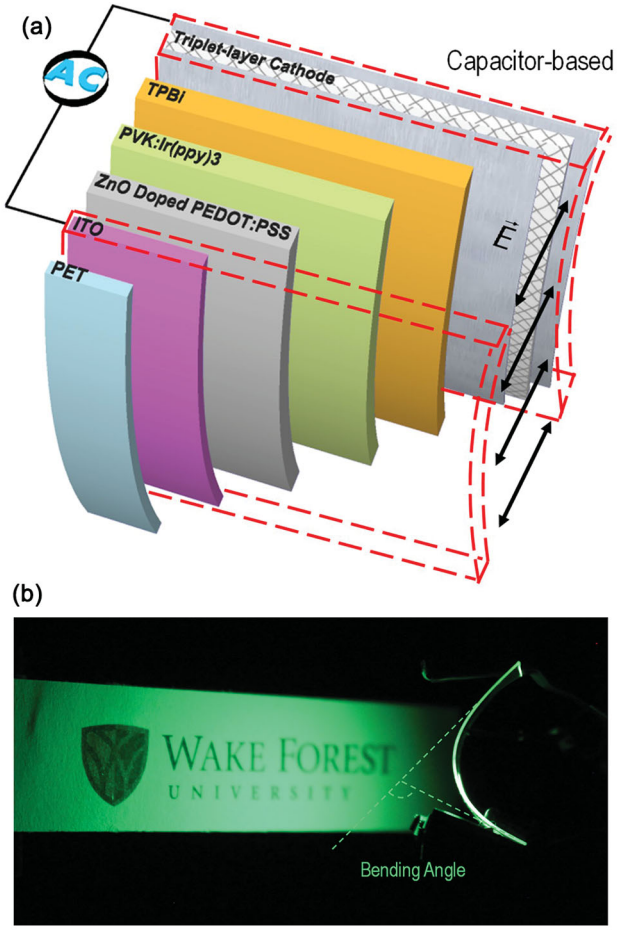

Figure 1. AC-driven organic EL device on flexible 1 in. × 1 in. plastic substrate. a) PET/ITO(100 nm)/PEDOT:PSS-doped ZnO NPs (80 nm)/PVK:Ir(ppy)3 (150 nm)/TPBi (35 nm)/triplet-layer cathode (≈200 nm). Electric fields due to AC driver in the capacitor-based device are changing in high frequency rather than pointing a unique direction. b) The definition of the bending angle used in this report.

AC-OEL devices can be found in our previous work.[2,7,13] In this work, poly(*N*-vinylcarbazole) (PVK):fac-tris(2-phenylpyridinato)iridium(III) ($Ir(ppy)_3$) is used as the electroluminescent layer with $Ir(ppy)_3$ as the triplet scavenging phosphorescent dye. 1,3,5-tris(2-*N*-Phenylbenzimidazolyl)benzene (TPBi) is an electron-rich (electronegative) dopant and transport layer used to help in charge generation at the interface to the emitter. The PEDOT serves an analogous function for hole injection. The multilayer composite electrode (metal/MWCNTs/metal) is deposited on the functional organic layers in a three step process before the devices are tested. This procedure is shown in **Figure 2** and is carried out as follows:

(a) A 50 nm layer of Al is predeposited through a shadow mask over the TPBi layer with a rate of 2 Å s^{-1} under high vacuum (≈2×10^{-7} Torr).
(b) A spray gun is used to deposit the MWCNT nanomatrix at different volumes of 0.5, 1.0, and 1.5 mL on the substrates. The MWCNTs are dispersed in acetone at a concentration of 0.2 mg mL^{-1} through ultrasonication.

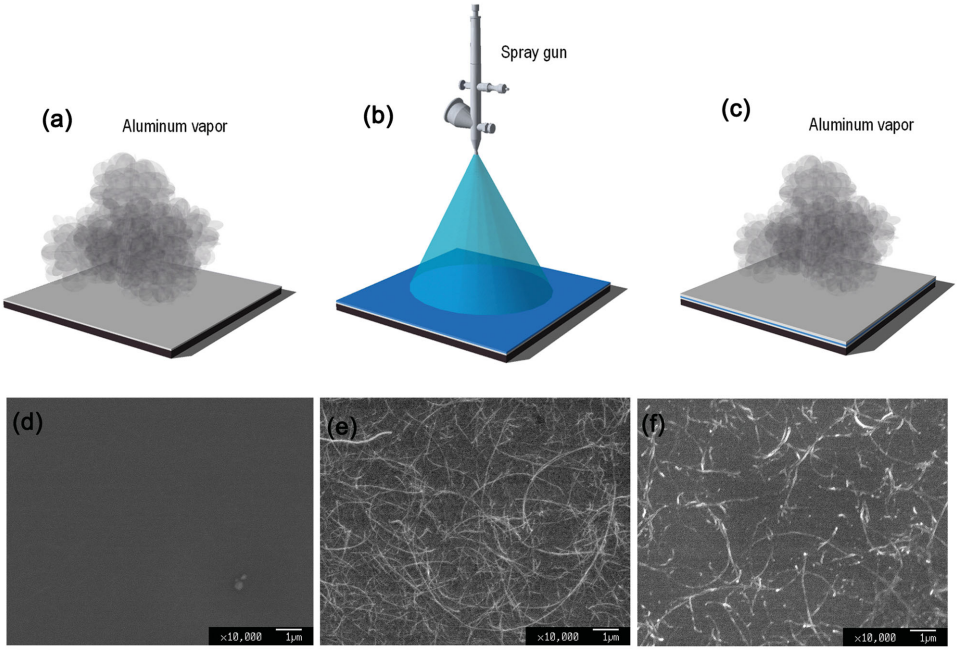

Figure 2. Multistep fabrication of triple-layer composite electrode. a) Thermal deposition of 50 nm Al layer. b) The formation of nanomatrix of MWCNTs with spraying. c) Top 100 nm Al layer coating. SEM images of multistep fabrication of triple-layer composite electrode. d) Al, e) Al/MWCNTs, f) Al/MWCNTs/Al, corresponding to (a–c).

(c) After postannealing in air for 10 min at 60° to evaporate excess solvent, the PET substrate is placed back into high vacuum for thermal evaporation of the final 100 nm of Al.

SEM images in Figure 2d–f show the three deposition steps in the fabrication and surface morphology of the Al/MWCNTs/Al composite cathode. The Al/MWCNTs/Al sandwich structure is asymmetric in that the bottom Al layer is flat and the top Al layer firmly coats the protruding MWCNTs network, which leaves a rough surface.

The property that we seek in this electrode is outstanding durability under multiple bending cycles. Generally, we would expect that the interlaced bundles of MWCNTs would exhibit high structural integrity and mechanical robustness as has already been reported in numerous applications.[53–55] We would also anticipate that mobile dislocations within the thin metal films will be pinned by the nanometer inclusions, thereby limiting failure due to work hardening of the film.

Electrically, it is well known that MWCNT mats can exhibit a rather high electrical conductivity at room temperature, but generally not as high as a metal like Al. This limits the application of the Al/MWCNTs/Al structure in DC-driven OLEDs since carrier injection efficiency is greatly affected by electrode resistance. MWCNTs also have a relatively high work function, between 4.40 and 4.95 eV, as compared to LiF/Al (2.6 eV), Mg (3.72 eV), Mg/Ag (4.12 eV), and Al (4.28 eV)).[56–58] This suggests pure nanotubes would be unsuitable to replace the metal as a top cathode in flexible lighting devices since there would exist a large electron injection barrier at the metal–semiconductor interface and the overall conductivity across the electrode would be inadequate. We add here that while the asymmetric AC-OEL devices with their unique capacitive nature, utilize a field-induced polarization current which contributes significantly to the light output, they also have some direct injection. Thus, even though lower carrier injection efficiency has less influence on the AC-OEL device's performance, it does have some. Furthermore, MWCNT mats' porous and low dimensional carbon structure produces a very low reflectivity surface for visible light (wavelength ≈400–700 nm). Therefore, clearly we want the mechanical properties of MWCNTs but not the electronic properties for this application.

However, a composite of nanotubes and a metal such as Al should result in a blending of the work functions of the two materials, while providing a surface with the reflectivity of the metal (for relatively small amounts of nanotubes) and finally the mechanical properties we seek, as described above. Unlike symmetric field-induced EL devices with two insulators or asymmetric El devices with a single insulator, the devices used in our studies are an asymmetric structure with a ZnO (semiconductor) gate. A unique feature of these asymmetric AC-OEL devices is that the contribution of injected charges has a nontrivial influence on the formation of excitons in the light emission layer, and thus the work function is of importance. The schematic of Al/MWCNTs/Al electrodes shown in Figure S1 in the Supporting Information suggests that electrons can easily be injected in the positive bias of AC cycles.

In order to avoid high temperature processing of a composite structure, our composite is formed by layering. This means the Al is exposed to air between the application of the MWNTs and the second layer, leading to a very thin alumina film. However, we expect that the mechanical properties to be dominated by the metal and the MWNTs. Figure 2d–f shows the formation of the composite layers using field emission SEM. We note here

Table 1. Summary of the performance of flexible organic AC-EL devices with different cathode structures.

Cathode structure	Turn-on RMS voltage [V]	Max. brightness [cd m^{-2}]	Max. power efficiency [lm W^{-1}]	Optimum frequency [Hz]
Al (150 nm)	5.76	4070	21.8	50k
Al (50 nm)/0.5 mL MWCNTs/Al (100 nm)	6.63	4050	22.2	60k
Al (50 nm)/1.0 mL MWCNTs/Al (100 nm)	10.71	3376	16.1	55k
Al (50 nm)/1.5 mL MWCNTs/Al (100 nm)	11.00	1982	7.3	50k

that the Al covered mat is relatively rough, but covered with Al, leaving behind a reflective film.

The AC-OEL device's flexibility was determined by measuring the performance parameters of brightness and lumens per watt as a function of the number of bends at a specified bend angle as defined in Figure 1b. Resistivity of the triple layer contact as well as microscopic analysis of the devices was carried out and correlated with the performance at specific bend conditions.

We first examine the effects of the triple-layer cathode on unbent geometries and these data are tabulated in **Table 1**. 0.5, 1.0, and 1.5 mL volumes of 0.2 wt% MWCNTs dispersions are used to create triple layer cathodes with different nanotube contents for comparison. Notice that the optimum operational frequency is where the AC driver is in resonance with the capacitive device for the maximum reactive power. This occurs at similar frequencies in all cases suggesting that the capacitance is roughly the same from device to device as we would expect. However, we note that the brightness decreases slightly with nanotubes in the metal layer while the turn-on voltage increases. This can be understood in terms of the relatively poor conductivity of MWCNTs (0.5–1 kΩ $\square^{-1}$)[59] compared to Al (≈0.3 Ω $\square^{-1}$). Quite simply, as more of the Al volume is replaced by the poorer conducting nanotubes, the overall conductivity of the system begins to drop proportionally and there is a potential drop now across the electrode. Consequently, the voltage drop seen across the emitting layer has gone down for a given voltage applied to the device. Electrical resistivity characteristics of Al electrode and Al/MWCNTs/Al are given in Figure S2 in the Supporting Information.

We expect three other factors have nonnegligible effects in raising the turn-on voltage while the light emission is reduced. The first of these is obviously due to the effects the increasing content of the nanotubes have on the reflectivity of the back cathode. The MWNTs are within 50 nm (less than the skin depth for Al) of the interface. So, while scattering generally helps output coupling in such devices, in this case the addition of a black absorber will surely reduce the output.

The second factor is the effect of increasing the work function of the cathode. In the AC-OEL, charge neutrality must be maintained throughout the power cycle. In the asymmetric configuration used here, this charge balance is established using makeup charge from the cathode—thereby requiring a low barrier to charge transport. If the injection barrier is raised, the compensating charge is hindered.

Finally, when the device is bent, there occurs a change in device capacitance. Since these devices operate at a resonance between the driver and the lamp capacitor, the frequency at which they should be driven for optimal light output changes as the capacitance changes. Bending can change the capacitance slightly and therefore move the device off of resonance. We expect this to yield a decrease in overall brightness since the device is being driven off of resonance. However, in this last case, we expect the capacitance to recover once the device has relaxed back (recovered) from the bending.

To minimize the negative effects of resistance in the MWCNT component of the composite, while examining their potential to enhance the robustness of device flexibility, AC-OEL devices with 0.5 mL of 0.2 wt% MWCNTs are chosen as our basis for comparison during bending. Clearly, from Table 1, AC-OEL devices with and without MWCNTs at this loading level in the cathode exhibited brightness's of the same order ($L_{max\_flat\_Al}$ = 3330 cd m^{-2} and $L_{max\_flat\_Al}$/MWCNTs/Al = 2700 cd m^{-2}. In **Figure 3**, we present the brightness data for Al only cathodes (Figure 3a) and compare to brightness for MWCNT cathodes (Figure 3b) for all voltages tested. When tested initially in an unbent state, the flat nanotube and flat Al only devices (open squares) are very nearly the same as would be expected, except for the slight offset associated with resistance in the cathode. Also notice that, in Figure 3c,d, the current–voltage characteristics associated with the flat devices without and with nanotubes respectively are linear and differ only by the resistance of the cathode.

A slight enhancement of the luminance is observed in both cases as the devices are bent from 0° to 120°. This is measuring the brightness at the center of curvature of the bend. The capacitance change of flexible AC-OEL devices with shape change of substrates (Figure S3 in the Supporting Information) should lead to a decrease in luminance as stated in our expectations above. Therefore, we attribute this slight increase to increased conductivity of the compressed electrodes induced by external mechanical deformation of the film and enhanced field density in this area. It should also be recognized that the output coupling of the light from the surface of the curved substrate during bending could be quite different from that of the flat state device, thereby leading to an observed increase in light output.

When the bent Al-based device is released, its brightness–voltage and current–voltage curves recover to their original shape, but the maximum luminance shifts from 4054 cd m^{-2} at 12.7 V at 90° to 3328 cd m^{-2} at 16.3 V in the recovered state. The lower optimal luminance and higher voltage required to achieve optimal luminance is consistent with the view that the cathode has formed cracks and deformations that have reduced its overall conductivity—thereby reducing the total voltage dropped across the emitter. This morphology change is confirmed in optical microscopy under 200× magnification shown in **Figure 4**. The formation of these cracks and creases

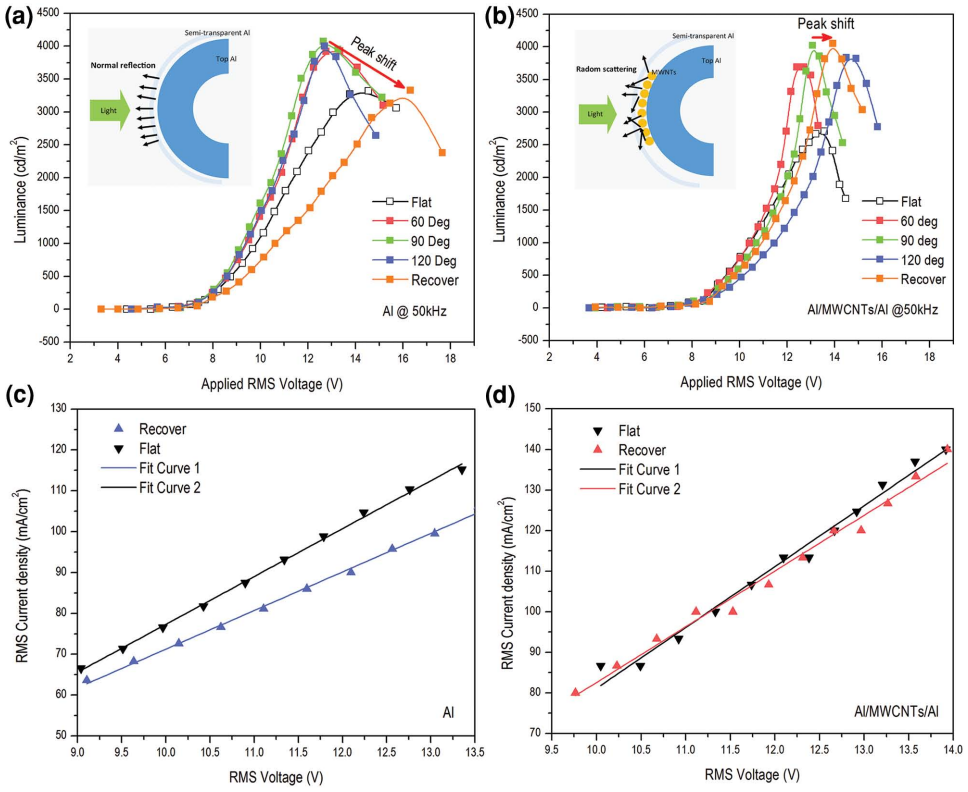

Figure 3. Performance of the green phosphorescent flexible organic AC-EL devices with and without MWCNTs driven at a frequency of 50 kHz during bending (flat, 60°, 90°, and 120°, recover). Luminance with a) Al or b) Al/MWCNT/Al as a function of voltage for flexible organic AC-EL devices. Red arrows represent the luminance peak shifts between the maximum luminance of the Al-based device and that of the Al/MWCNT/Al-based device. c,d) RMS current density versus RMS voltage characteristics of flexible organic AC-OEL devices before and after bending.

in Figure 4a is an irreversible process, and thus poor conductivity results when the device is flattened after severe bends.

In contrast, consistent EL performance of MWCNT-based devices is observed with bending and recovery. A small luminance peak shift from 4002 cd m^{-2} at 13.1 V at 90° to 4060 cd m^{-2} at 13.9 V in the recovered state, as shown in Figure 3b, is seen, but peak shape as well as optimal luminance is, intriguingly, maintained. We attribute this to the mechanical properties of the networked structure of the Al/MWCNT/Al electrode. The composite cathode keeps the surface morphology crack-free even under large-angle bends since dislocations within the Al are being pinned and additional some stress is taken by the nanotubes—not the malleable metal. Again, optical micrographs at 200× magnification confirms the morphology as seen in Figure 4b. However, the EL performances in MWCNT-based devices do show a slight shift in the voltage where the maximum luminance occurs under different bending angles compared with Al-based devices. We attribute the difference to the reflections on back electrodes: normal reflection to Al and random scattering to Al/MWCNTs/Al (insets in Figure 3a,b).

There is one final issue. AC-OEL devices can be thought of as a light emitting capacitor. High-frequency electric fields induce a polarization current within the device to generate light. Therefore, the electrodes must be just as highly conductive and homogeneous as in the case of OLEDs. Creases and voids in the Al film due poor mechanical properties can cause local potential variations in the device which show up as brightness inhomogeneity. The network of MWCNTs clearly imparts some mechanical stability on the Al film during bending leading to uniformity in the composite cathodes spreading resistance. To see this point more clearly, RMS current density versus the RMS voltage (J–V) of Al-based devices and composite electrode-based devices are compared in Figure 3c,d. The difference between J–V curves of Al-based case before and after a full cycle of 120° bend is an unmistakable increase in the resistivity (slope of the line). However, the J–V characteristics of Al/MWCNTs/Al device before and after bending are nearly identical suggesting not very much permanent morphological change has taken place.

In measuring the power efficiency of the devices, we use the standard convention of measuring the current voltage and the phase angle between them.[1] For both cathode types (with and without MWCNTs), the overall power efficiency of flat devices is quite similar except for small fluctuations from device to device. However, in **Figure 5**, we show what happens to the power efficiency of composite cathode devices as compared to pure Al cathodes under bending. For example, a pure Al cathode device flat that has not been bent achieves ≈22 lm W^{-1} at 3250 cd m^{-2} but yields only 18 lm W^{-1} at 3250 cd m^{-2} after bending once to 120° and fully relaxing back. Notice that this is not the case for the composite cathode devices that track almost exactly in its recovery from 120° bending.

Importantly, the EL spectra of devices with MWCNT cathodes taken at different bending angles and displayed in Figure 4 in

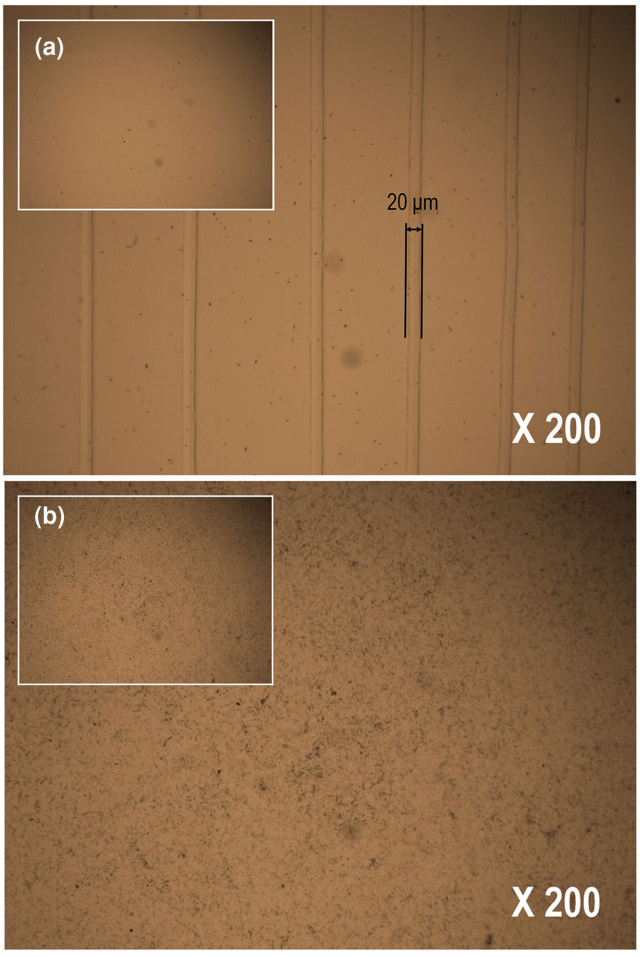

Figure 4. Metallurgical microscopy images of top electrodes in flexible organic AC-EL devices before (insets) and after a full cycle of 120° bending. a) Al (150 nm) electrode shows 20 μm width creases due to bending. b) Al (50 nm)/MWCNT/Al (100 nm) composite electrode shows outstanding mechanical property in bending.

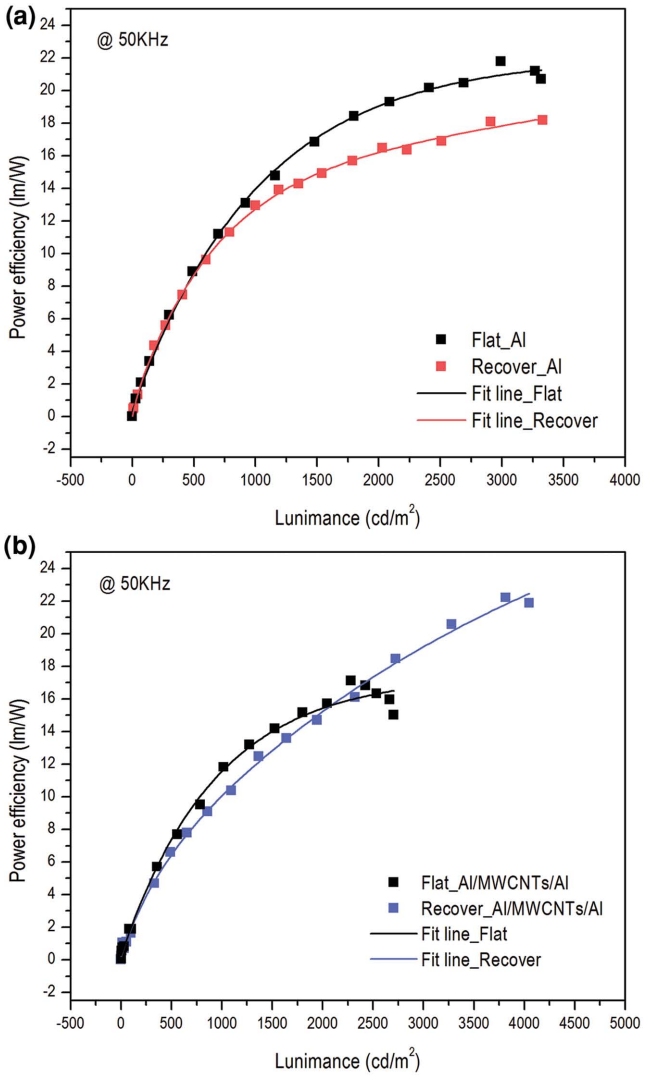

Figure 5. Power efficiencies with a) Al or b) Al/MWCNT/Al as a function of luminance for flexible AC-OEL devices.

the Supporting Information do show subtle differences. Most notably, the recovered spectra from a previously bent device seem to suggest some damage is done to the device, perhaps delamination at the interfaces. However, it is important to realize that this is for one set of loadings only and optimization of MWCNT content has yet to be completely optimized.

Iterative bending tests on the AC-OEL devices were performed holding the bending angle at a constant 90° (radius of curvature ≈9 mm), for each bend. As shown in **Figure 6**a, the luminance remains very stable in devices with MWCNT composite electrodes, requiring over 500 bending cycles to drop to half of the initial luminance (1250 cd m^{-2}). In comparison, devices with pure Al electrodes exhibit a luminance drop of the same magnitude (half of the initial brightness (1270 cd m^{-2})) with only 50 bending cycles. The inset in Figure 6a shows an illuminated AC-OEL device after 1000 bending cycles.

A voltage sweep at 50 kHz driving frequency was made before and after 1300 bending cycles and *L*–*J*–*V* characteristics are shown in Figure 6b,c, respectively. Compared with identical performances before bends (Figure 6b), after continuous 1300 bending cycles the device with an MWCNT composite cathode shows a luminance and current density of over 1290 cd m^{-2} at 133 mA cm^{-2} while the Al-based cathode device only produced 600 cd m^{-2} at 93 mA cm^{-2} (Figure 6c). The superior mechanical reliability of the AC-OEL device with an Al/MWCNT/Al composite cathode, again, can be attributed to the strong mechanical strength of the MWCNT network together with the nanoinclusions ability to pin mobile defects in the metal films.

3. Conclusion

We have presented the use of a composite cathode made up of an Al/MWCNTs/Al trilayer, on flexible organic light emitting devices. Our results demonstrate that making use of such a cathode structure can impart mechanical stability to the flexible device allowing for repeated bending without significant loss of brightness or power efficiency. We interpret these results as a transfer of stress to the nanotube components

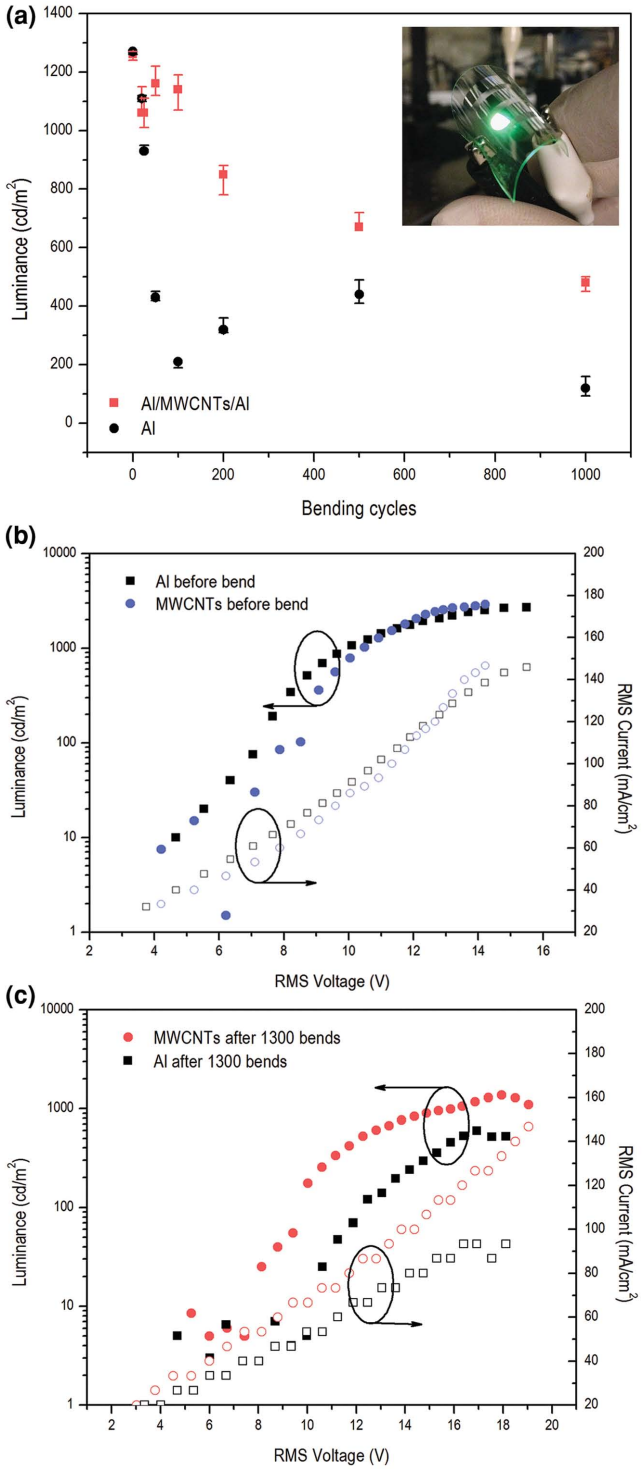

Figure 6. Bending test of flexible organic AC-EL devices with and without MWCNT nanonetwork modification. a) Luminance as a function of the number of cycles (0, 20, 25, 50, 100, 200, 500, and 1000). The inset shows the photograph of the flexible device with MWCNTs after 1000 bends. Luminance–current density–voltage characteristic of flexible organic AC-OEL devices b) before and c) after 1300 cycles of bend.

of the film along with the pinning of mobile defects in the film both of which prevents the formation of voids, cracks, and morphological defects that typically increase the films resistance with bending. Moreover, we show that the optical and electrical properties of such composite films are compatible with these applications for both AC-OEL as well as OLEDs. We believe that this suggests that the triple-layer composite electrode (metal/nanotubes or nanowires/metal) is a reliable alternative electrode approach for commercial flexible organic lighting devices of the future.

4. Experimental Section

Materials and Device Fabrication: All devices were fabricated on a PET substrate with a precoated 100 nm ITO film with a sheet resistance of ≈10 Ω $\square^{-1}$. The plastic substrates were cleaned in an ultrasonic bath with acetone followed by methanol and isopropanol for 1 h each. The flexible ITO substrates subsequently were dried in a vacuum oven for 2 h and treated with UV-ozone for 15 min. ZnO NPs aqueous solution (50 wt%, average diameter ≈35 nm, Aldrich) was purchased. Poly(3,4-ethylenedioxythiophene)-poly(styrenesulfonate) (PEDOT:PSS, 1.5 wt%, Heraeus) was mixed with ZnO NPs at a concentration of 36 wt% (ZnO to PEDOT:PSS). Ammonium hydroxide was added into PEDOT:PSS to keep the ZnO NP dispersed. The emission layer consisted of a blend of poly(*N*-vinylcarbazole) (PVK) as a cohost and 10 wt% fac-tris(2-phenylpyridinato)iridium(III) ($Ir(ppy)_3$) as the dopant. The emitting layers were obtained by spin coating the 18 mg mL^{-1} PVK:$Ir(ppy)_3$ blend in chlorobenzene at 2000 rpm. As an electron injection layer, TPBi is dissolved in a mixture of formic acid and water (5:1) and spin cast at 4000 rpm before moving to a heated vacuum oven for 30 min. For fabrication of the Al/MWCNTs/Al electrodes, 50 nm of Al was deposited initially via thermal evaporation at a pressure of about 2×10^{-7} Torr with a rate of 2 Å s^{-1}. A 0.2 mg mL^{-1} dispersion of MWCNTs was made in acetone after 15 min of ultrasonication and then sprayed by an airbrush powered by nitrogen gas at 5 psi. The distance between spray gun nozzle and the surface of substrate was set to 10 cm to avoid the formation of large aggregated droplets on the substrate. Then, another 100 nm layer of Al was deposited after the flexible substrate was sent back to high vacuum. The active area of the flexible organic AC-EL pixels was 0.15 cm^2.

Device Electroluminescence Measurement: The AC-driven field-induced polymer EL devices in this report are measured in ambient air at atmospheric pressure and room temperature (25 °C) without sealing. A 200 MHz function/arbitrary waveform generator (Agilent 33220A) connected to a Trek PZD700A M/S amplifier provides a sinusoidal signal with suitable voltage and frequency. Voltage, current, and phase angle are recorded from a Tektronix TPS 2024B oscilloscope. An ILT 1400-A photometer (International Light Technologies) is used to measure the out-coupling luminance. EL spectra were collected using an ILT 950 spectroradiometer (International Light Technologies). The time resolved AC electroluminescence response is recorded with a fast photo diode. The entire system is connected and controlled by a computer. In order to maintain accurate and reliable measurements of luminance and efficiency, each turn-on measurement of the pixels was integrated over 2000 ms and averaged five times instead of fast sweeping for good-looking curves. We note here that during the time frame of our measurements the lamps in this study were stable and showed no signs of deterioration.

SEM and Optical Images: A scanning electron microscope (SEM, JEOL 6330) was utilized to measure the morphology of the composite electrode for each step of the fabrication process. The surface morphology of organic AC-EL devices with Al cathode or Al/MWCNTs/Al was measured by a metallurgical microscope (Olympus BX60M) before and after a full cycle of 120° bending.

Supporting Information

Supporting Information is available from the Wiley Online Library or from the author.

Acknowledgements

The authors acknowledge the Wake Forest Center for Nanotechnology and Molecular Materials for generous funding and use of facilities and instrumentation.

Received: March 17, 2015
Revised: April 25, 2015
Published online: June 10, 2015

[1] A. Perumal, M. Fröbel, S. Gorantla, T. Gemming, B. Lüssem, J. Eckert, K. Leo, *Adv. Funct. Mater.* **2012**, *22*, 210.
[2] Y. Chen, Y. Xia, G. M. Smith, D. L. Carroll, *Adv. Mater.* **2014**, *26*, 8133.
[3] J. Sung, Y. S. Choi, S. J. Kang, S. H. Cho, T.-W. Lee, C. Park, *Nano Lett.* **2011**, *11*, 966.
[4] T. Yamao, Y. Shimizu, K. Terasaki, S. Hotta, *Adv. Mater.* **2008**, *20*, 4109.
[5] V. Wood, M. J. Panzer, D. Bozyigit, Y. Shirasaki, I. Rousseau, S. Geyer, M. G. Bawendi, V. Bulovi , *Nano Lett.* **2011**, *11*, 2927.
[6] L. Zhang, H. Nakanotani, K. Yoshida, C. Adachi, *Org. Electron.* **2014**, *15*, 1815.
[7] Y. Chen, Y. Xia, G. M. Smith, H. Sun, D. Yang, D. Ma, Y. Li, W. Huang, D. L. Carroll, *Adv. Funct. Mater.* **2014**, *24*, 2677.
[8] M. Fröbel, A. Perumal, T. Schwab, M. C. Gather, B. Lüssem, K. Leo, *Org. Electron.* **2013**, *14*, 809.
[9] A. Perumal, B. Lüssem, K. Leo, *Org. Electron.* **2012**, *13*, 1589.
[10] S. H. Cho, J. Sung, I. Hwang, R. H. Kim, Y. S. Choi, S. S. Jo, T. W. Lee, C. Park, *Adv. Mater.* **2012**, *24*, 4540.
[11] Y. Chen, Y. Xia, G. M. Smith, C. a. Hewitt, Q. Fu, Y. Liu, H. Sun, D. Ma, Y. Gu, C. Yang, Y. Mei, D. L. Carroll, *Org. Electron.* **2014**, *15*, 182.
[12] Y. Chen, Y. Xia, G. M. Smith, Y. Gu, C. Yang, D. L. Carroll, *Appl. Phys. Lett.* **2013**, *102*, 013307.
[13] Y. Chen, Y. Xia, H. Sun, G. M. Smith, D. Yang, D. Ma, D. L. Carroll, *Adv. Funct. Mater.* **2014**, *24*, 1501.
[14] Z. B. Wang, M. G. Helander, J. Qiu, D. P. Puzzo, M. T. Greiner, Z. M. Hudson, S. Wang, Z. W. Liu, Z. H. Lu, *Nat. Photonics* **2011**, *5*, 753.
[15] T.-H. Han, Y. Lee, M.-R. Choi, S.-H. Woo, S.-H. Bae, B. H. Hong, J.-H. Ahn, T.-W. Lee, *Nat. Photonics* **2012**, *6*, 105.
[16] B. R. Lee, E. D. Jung, J. S. Park, Y. S. Nam, S. H. Min, B.-S. Kim, K.-M. Lee, J.-R. Jeong, R. H. Friend, J.-S. Kim, S. O. Kim, M. H. Song, *Nat. Commun.* **2014**, *5*, 4840.
[17] H. Chang, G. Wang, A. Yang, X. Tao, X. Liu, Y. Shen, Z. Zheng, *Adv. Funct. Mater.* **2010**, *20*, 2893.
[18] K. Kwak, K. Cho, S. Kim, *Sci. Rep.* **2013**, *3*, 2787.
[19] M. D. Ho, D. Kim, N. Kim, S. M. Cho, H. Chae, *ACS Appl. Mater. Interfaces* **2013**, *5*, 12369.
[20] S. R. Forrest, *Nature* **2004**, *428*, 911.
[21] C. Adachi, M. a. Baldo, M. E. Thompson, S. R. Forrest, *J. Appl. Phys.* **2001**, *90*, 5048.
[22] M. A. Baldo, S. R. Forrest, *Nature* **1998**, *395*, 151.
[23] Y. Kawamura, K. Goushi, J. Brooks, J. J. Brown, H. Sasabe, C. Adachi, *Appl. Phys. Lett.* **2005**, *86*, 071104.
[24] M. Baldo, M. Thompson, S. Forrest, *Nature* **2000**, *403*, 750.
[25] H. Uoyama, K. Goushi, K. Shizu, H. Nomura, C. Adachi, *Nature* **2012**, *492*, 234.
[26] C.-H. Kim, J. Shinar, *Appl. Phys. Lett.* **2002**, *80*, 2201.
[27] V.-E. Choong, S. Shi, J. Curless, C.-L. Shieh, H.-C. Lee, F. So, J. Shen, J. Yang, *Appl. Phys. Lett.* **1999**, *75*, 172.
[28] G. He, M. Pfeiffer, K. Leo, M. Hofmann, J. Birnstock, R. Pudzich, J. Salbeck, *Appl. Phys. Lett.* **2004**, *85*, 3911.
[29] J. Kido, M. Kimura, K. Nagai, *Science* **1995**, *267*, 1332.
[30] X. M. Ding, L. M. Hung, L. F. Cheng, Z. B. Deng, X. Y. Hou, C. S. Lee, S. T. Lee, *Appl. Phys. Lett.* **2000**, *76*, 2704.
[31] J. Huang, M. Pfeiffer, A. Werner, J. Blochwitz, K. Leo, S. Liu, *Appl. Phys. Lett.* **2002**, *80*, 139.
[32] J. C. Scott, *J. Vac. Sci. Technol. A* **2003**, *21*, 521.
[33] S. J. Su, T. Chiba, T. Takeda, J. Kido, *Adv. Mater.* **2008**, *20*, 2125.
[34] W.-Y. Wong, C.-L. Ho, *J. Mater. Chem.* **2009**, *19*, 4457.
[35] S. De, T. M. Higgins, P. E. Lyons, E. M. Doherty, P. N. Nirmalraj, W. J. Blau, J. J. Boland, J. N. Coleman, *ACS Nano* **2009**, *3*, 1767.
[36] S. Nanowire, L. Hu, H. S. Kim, J. Lee, P. Peumans, Y. Cui, *ACS Nano* **2010**, *4*, 2955.
[37] J. Krantz, T. Stubhan, M. Richter, S. Spallek, I. Litzov, G. J. Matt, E. Spiecker, C. J. Brabec, *Adv. Funct. Mater.* **2013**, *23*, 1711.
[38] J. Y. Lee, S. T. Connor, Y. Cui, P. Peumans, *Nano Lett.* **2008**, *8*, 689.
[39] S. Ju, J. Li, J. Liu, P. C. Chen, Y. G. Ha, F. Ishikawa, H. Chang, C. Zhou, A. Facchetti, D. B. Janes, T. J. Marks, *Nano Lett.* **2008**, *8*, 997.
[40] L. Zhou, H. Xiang, S. Shen, Y. Li, J. Chen, H. Xie, I. A. Goldthorpe, L. Chen, S. Lee, J. Tang, *ACS Nano* **2014**, *8*, 12796.
[41] G. Eda, Y.-Y. Lin, S. Miller, C.-W. Chen, W.-F. Su, M. Chhowalla, *Appl. Phys. Lett.* **2008**, *92*, 233305.
[42] A. K. Geim, K. S. Novoselov, *Nat. Mater.* **2007**, *6*, 183.
[43] X. Li, G. Zhang, X. Bai, X. Sun, X. Wang, E. Wang, H. Dai, *Nat. Nanotechnol.* **2008**, *3*, 538.
[44] J. C. Meyer, a K. Geim, M. I. Katsnelson, K. S. Novoselov, T. J. Booth, S. Roth, *Nature* **2007**, *446*, 60.
[45] X. Wang, L. Zhi, K. Müllen, *Nano Lett.* **2008**, *8*, 323.
[46] Q. Cao, Z.-T. Zhu, M. G. Lemaitre, M.-G. Xia, M. Shim, J. A. Rogers, *Appl. Phys. Lett.* **2006**, *88*, 113511.
[47] L. Hu, D. S. Hecht, G. Grüner, *Nano Lett.* **2004**, *4*, 2513.
[48] Z. Wu, Z. Chen, X. Du, J. M. Logan, J. Sippel, M. Nikolou, K. Kamaras, J. R. Reynolds, D. B. Tanner, A. F. Hebard, A. G. Rinzler, *Science* **2004**, *305*, 1273.
[49] B. Dan, G. C. Irvin, M. Pasquali, *ACS Nano* **2009**, *3*, 835.
[50] J. Lee, H. Shin, Y. Noh, S. Na, H. Kim, *Sol. Energy Mater. Sol.* **2013**, *114*, 15.
[51] J. Xu, L. Zhang, J. Zhong, H. Lin, *Opt. Rev.* **2012**, *19*, 358.
[52] M. Mazzeo, F. Mariano, A. Genco, S. Carallo, G. Gigli, *Org. Electron.* **2013**, *14*, 2840.
[53] G. Toth, J. Mäklin, N. Halonen, J. Palosaari, J. Juuti, H. Jantunen, K. Kordas, W. G. Sawyer, R. Vajtai, P. M. Ajayan, *Adv. Mater.* **2009**, *21*, 2054.
[54] M. S. Dresselhaus, *Nature* **2004**, *432*, 959.
[55] J. Chen, A. Minett, Y. Liu, C. Lynam, P. Sherrell, C. Wang, G. Wallace, *Adv. Mater.* **2008**, *20*, 566.
[56] L. Ma, Organic light-emitting diode with enhanced efficiency *US 20130069044 A1*, **2011**.
[57] H. Ago, T. Kugler, F. Cacialli, W. R. Salaneck, M. S. P. Shaffer, A. H. Windle, R. H. Friend, *J. Phys. Chem. B* **1999**, *103*, 8116.
[58] M. Shiraishi, M. Ata, *MRS Proc.* **2000**, *633*, 1913.
[59] D. Jung, K. H. Lee, D. Kim, D. Burk, L. J. Overzet, G. S. Lee, *Jpn. J. Appl. Phys.* **2013**, *52*, 03BC03.